Modulated light transmission through a subwavelength slit at early stage

Jian-Shiung Hong,[1] **Alexander Ewen Chen,**[2] **and Kuan-Ren Chen**[3,*]

[1]*Department of Photonics, National Cheng Kung University, 1 University Road, Tainan 70101, Taiwan*

[2]*Department of Electrical Engineering, The Pennsylvania State University, University Park, PA 16802, USA*

[3]*Department of Physics, National Cheng Kung University, 1 University Road, Tainan 70101, Taiwan*

[*]*chenkr@mail.ncku.edu.tw*

Abstract: We simulate the early dynamics of enhanced light transmission through a subwavelength metallic slit and find that the amplitude of the transmitted light can be modulated. To understand this novel phenomenon and underlying physics, we develop a new analytical model. The field of each light period is considered as an individual unit. Each field is partially transmitted through the slit as the first subunit. The portion reflected from the exit interface travels a round trip in the slit and then partially exits again as the second subunit. There may be a gap in time between these two subunits. This process repeats so as to produce a subunit train, which is verified by the simulation of an incident sinusoidal pulse of one light period. When the wave units are continuous, the superposition of the trains produces the observed light. While the round-trip time is an integer multiple of the light period, the modulation period is the same. Besides academic importance, this study may be applicable to photonics with short laser pulses.

OCIS codes: (050.6624) Subwavelength structures; (050.2230) Fabry-Perot; (260.3160) Interference; (320.2250) Femtosecond phenomena.

References and links

1. T. W. Ebbesen, H. J. Lezec, H. F. Ghaemi, T. Thio, and P. A. Wolff, "Extraordinary optical transmission through sub-wavelength hole arrays," Nature **391**, 667–669 (1998).
2. K. F. MacDonald, Z. L. Samson, M. I. Stockman, and N. I. Zheludev, "Ultrafast active plasmonics," Nature Photon. **3**, 55–58 (2009).
3. W. Zhang, L. Huang, C. Santschi, and O. J. Martin, "Trapping and sensing 10 nm metal nanoparticles using plasmonic dipole antennas," Nano Lett. **10**, 1006–1011 (2010).
4. J. N. Anker, W. P. Hall, O. Lyandres, N. C. Shah, J. Zhao, and R. P. Van Duyne, "Biosensing with plasmonic nanosensors," Nature Mater. **7**, 442–453 (2008).
5. H. A. Atwater and A. Polman, "Plasmonics for improved photovoltaic devices," Nature Mater. **9**, 205–213 (2010).
6. L. Novotny and N. van Hulst, "Antennas for light," Nature Photon. **5**, 83–90 (2011).
7. T. Xu, Y.-K. Wu, X. Luo, and L. J. Guo, "Plasmonic nanoresonators for high-resolution colour filtering and spectral imaging," Nat. Commun. **1**, 59 (2010).
8. H. J. Lezec, A. Degiron, E. Devaux, R. A. Linke, L. Martín-Moreno, F. J. García-Vidal, and T. W. Ebbesen, "Beaming light from a subwavelength aperture," Science **297**, 820–822 (2002).
9. F. J. García-Vidal, L. Martín-Moreno, H. J. Lezec, and T. W. Ebbesen, "Focusing light with a single subwavelength aperture flanked by surface corrugations," Appl. Phys. Lett. **83**, 4500 (2003).
10. K. R. Chen, "Focusing of light beyond the diffraction limit of half the wavelength," Opt. Lett. **35**, 3763–3765 (2010).

#234872 - $15.00 USD Received 17 Feb 2015; revised 27 Mar 2015; accepted 31 Mar 2015; published 9 Apr 2015

11. K. R. Chen, W. H. Chu, H. C. Fang, C. P. Liu, C. H. Huang, H. C. Chui, C. H. Chuang, Y. L. Lo, C. Y. Lin, H. H. Hwung, and A. Y. G. Fuh, "Beyond-limit light focusing in the intermediate zone," Opt. Lett. **36**, 4497–4499 (2011).
12. W. L. Barnes, A. Dereux, and T. W. Ebbesen, "Surface plasmon subwavelength optics," Nature **424**, 824–830 (2003).
13. P. Lalanne and J. P. Hugonin, "Interaction between optical nano-objects at metallo-dielectric interfaces," Nature Phys. **2**, 551–556 (2006).
14. J. B. Pendry, L. Martín-Moreno, and F. J. García-Vidal, "Mimicking surface plasmons with structured surfaces," Science **305**, 847–848 (2004).
15. F. L. Neerhoff and G. Mur, "Diffraction of a plane electromagnetic wave by a slit in a thick screen placed between two different media," Appl. Sci. Res. **28**, 73–88 (1973).
16. E. Betzig, A. Harootunian, A. Lewis, and M. Isaacson, "Near-field diffraction by a slit - implications for super-resolution microscopy," Appl. Opt. **25**, 1890–1900 (1986).
17. R. F. Harrington and D. T. Auckland, "Electromagnetic transmission through narrow slots in thick conducting screens," IEEE Trans. Antennas Propag. **AP-28**, 616–622 (1980).
18. S. Astilean, P. Lalanne, and M. Palamaru, "Light transmission through metallic channels much smaller than the wavelength," Opt. Commun. **175**, 265–273 (2000).
19. Y. Takakura, "Optical resonance in a narrow slit in a thick metallic screen," Phys. Rev. Lett. **86**, 5601–5603 (2001).
20. J. Bravo-Abad, L. Martín-Moreno, and F. J. García-Vidal, "Transmission properties of a single metallic slit: From the subwavelength regime to the geometrical-optics limit," Phys. Rev. E **69**, 026601 (2004).
21. R. Gordon, "Light in a subwavelength slit in a metal: Propagation and reflection," Phys. Rev. B **73**, 153405 (2006).
22. M. Mechler, O. Samek, and S. V. Kukhlevsky, "Enhanced transmission and reflection of few-cycle pulses by a single slit," Phys. Rev. Lett. **98**, 163901 (2007).
23. S. V. Kukhlevsky, M. Mechler, L. Csapo, and K. Janssens, "Near-field diffraction of fs and sub-fs pulses: super resolution of nsom in space and time," Phys. Lett. A **319**, 439–447 (2003).
24. J. Wuenschell and H. K. Kim, "Excitation and propagation of surface plasmons in a metallic nanoslit structure," IEEE Trans. Nanotechnol. **7**, 229–236 (2008).
25. X. Wang, X. G. Zhang, Q. Yu, and B. N. Harmon, "Multiple-scattering theory for electromagnetic waves," Phys. Rev. B **47**, 4161–4167 (1993).
26. K. Y. Kim, Y. K. Cho, H.-S. Tae, and J.-H. Lee, "Light transmission along dispersive plasmonic gap and its subwavelength guidance characteristics," Opt. Express **14**, 320–330 (2006).

1. Introduction

The extraordinary optical transmission (EOT) through a subwavelength hole array in a metallic film [1] is a fundamental scientific topic in wave mechanics and inspires researchers in the area of plasmonics to explore the possibility of applications on optical devices, such as ultrafast active plasmonics [2], particle trapping [3], bio-sensing [4], plasmonic solar cells [5], optical antennas [6], color filters [7], and light shape manipulation [8–11], etc. A single subwavelength slit is the simplest configuration to understand the fundamental mechanism and its related optical properties. For simplicity, the metal can be considered as a perfect electric conductor (PEC) for the investigation of interesting transmission phenomena. Although PEC does not support surface plasmons (SPs) [12, 13], the wave-SP-like interaction can still be studied with structured PEC because of the so-called "spoof SPs" [14].

In the last few decades, extensive theoretical works have been carried out for understanding the steady light transmission through this kind of configuration. For instance, Neerhoff and Mur [15] introduced the Green's theorem for the calculation of light transmission through a slit with the width larger than the incident wavelength; Betzig et al. [16] confirmed its accuracy when the slit is of subwavelength scale. Harrington and Auckland [17] proposed an equivalent transmission line model for this problem. Both theories predict the transmitted light intensity varying periodically with the film thickness. In fact, the slit can be considered as an open cavity to allow a Fabry-Pérot-like resonance resultant from the reflected waves traveling back and forth in the slit [18]. The resonance has also been theoretically investigated by a mode expansion method [19, 20], as well as the phase shift of the reflection inside the slit [21].

#234872 - $15.00 USD Received 17 Feb 2015; revised 27 Mar 2015; accepted 31 Mar 2015; published 9 Apr 2015

Mechler et al. [22] analyzed the transmission of Gaussian pulses with only a few light periods and pointed out that there are three regimes of resonant excitation according to their temporal pulse widths. In fact, the time-dependent analysis was obtained by the inverse Fourier transform from the solution of Neerhoff and Mur at each frequency, i.e., solving the phasor of the time-harmonic electric and magnetic fields from Maxwell's equations [23].

In this article, periodical variation of the transmitted energy as a function of thickness and transmission spectra due to Fabry-Pérot-like resonance for a subwavelength slit are demonstrated from monochromatic sources or a sinusoidal pulse of one light period in a finite-difference time-domain (FDTD) simulation system. With a monochromatic light, we find that the transmitted electric field through the configuration can be monotonically increased at the early stage. In fact, the increment is periodically modulated before the amplitude is saturated. The saturation time increases with the film thickness and requires at least four wave periods of the light wave, which is comparable to the time scale of a femtosecond (fs) laser pulse. We propose a new analytical model in which the wave field generated in each light period is considered as an individual unit. Each wave unit can produce a train of subunits due to partial reflections within the slit at its entrance and exit interfaces as well as the propagation in between. The repeating process is verified by the sinusoidal pulse illumination. The superposition of the wave units at the observation location yields the wave fields that agree well with the simulation results. This model illuminates the underlying new physics.

In section 2, we show the Fabry-Pérot-like resonance for the configuration and the simulation results for the increment and the modulation of the electric fields. Section 3 gives the novel analytical model. We obtain the parameters needed by the model from the FDTD simulation in section 4. In section 5, the modeling results are compared with those of the simulation. Section 6 is the discussions on the numerical issues and the implication of our model for ultrashort applications. Section 7 is the summary.

2. The Fabry-Pérot-like resonance and modulated light transmission at early stage

Consider a subwavelength slit perforated in a PEC film, as shown in Fig. 1. The slit width $2s$ is 40 nm and the film thickness h will vary. A p-polarized wave source of wavelength $\lambda_0 = 560$ nm is located at a distance of one wavelength away ($d = \lambda_0$) to illuminate the film. The light period is $T = \lambda_0/c_0 = 1.87$ fs, where c_0 is the light speed in vacuum.

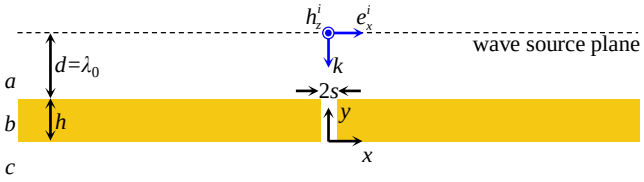

Fig. 1. Schematic of the simulated structure. A p-polarized wave with its wavelength of $\lambda_0 = 560$ nm is generated at a distance of one λ_0 away from the top of the PEC. The slit width $2s$ is 40 nm while the film thickness h will vary. In the model, the space is divided into three areas of a, b, and c.

In the FDTD simulation, the cell size of both directions is 5 nm, and the time-step is $0.005T$. Perfectly matched layers (PMLs) are used as the boundary condition. The PEC is simulated by the Drude model with a sufficiently high plasma frequency ω_p ($= 1.0 \times 10^{30}$ Hz) and the damping coefficient set to be zero.

The time dependence of the source is given as $\sin(\omega_0 t)$ at $y = h + d$, where ω_0 is the angular frequency. Hence, the electric field of the incident plane wave is in the x-direction and

#234872 - $15.00 USD Received 17 Feb 2015; revised 27 Mar 2015; accepted 31 Mar 2015; published 9 Apr 2015

taken as the imaginary part of the complex electric field, i.e., $e_x^i(x,y,t) = \mathrm{Im}\{E_0 e^{i(k_0 y' + \omega_0 t)}\} = E_0 \sin(k_0 y' + \omega_0 t)$, where $y' = y - (h+d)$, k_0 is the wave number in vacuum, and E_0 is the amplitude normalized to unity. The magnetic field in the z-direction is $h_z^i(x,y,t) = e_x^i(x,y,t)/\eta_0$, where η_0 is the impedance of vacuum, which is also normalized to unity.

When the incident wave propagates to the film, it will be transmitted through the slit and diffracted as a cylindrical wave. At an observation location $(x = 0, y)$ far from the slit in region c , we can define the normalized transmitted energy flux as

$$P(\omega_0) = \frac{\pi|y|}{sE_0^2 T} \int_{t_f - T}^{t_f} e_x(0,y,t) h_z(0,y,t) dt, \tag{1}$$

where $e_x(0,y,t)$ and $h_z(0,y,t)$ are the simulated electric and magnetic fields, respectively, and $t_f = 40T$ is the FDTD simulation time to ensure the time-harmonic oscillation of the fields; in the definition, the transmitted energy flux is the time-averaged Ponyting vector multiplying $\pi|y|$ while the incident energy flux is $2s(\frac{1}{2}E_0^2) = sE_0^2$. Figure 2 shows the obtained $P(\omega_0)$ at $y = -\lambda_0$, where h varies from 50 nm to 800 nm in a step of 5 nm. The energy flux varies periodically because of Fabry-Pérot-like resonance [19, 20]. At optimized transmission, the corresponding film thicknesses h's are 205 nm, 470 nm, and 730 nm, and the obtained energy fluxes are 4.28, 4.26, and 4.28, respectively.

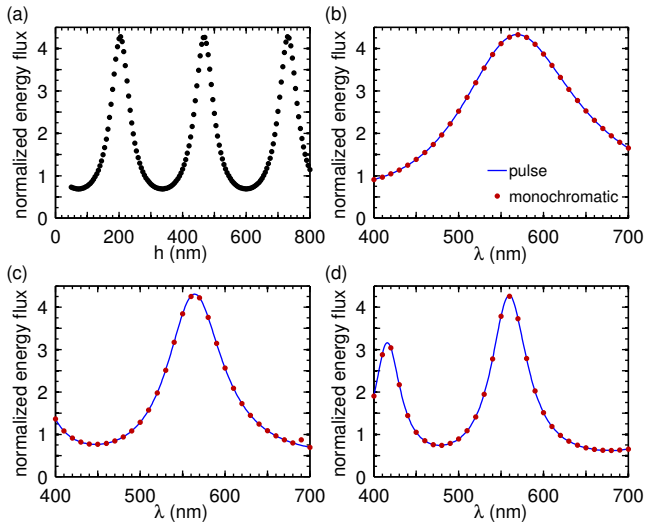

Fig. 2. Normalized energy flux as a function of the film thickness h (a), and as a function of wavelength when $h = 205$ nm (b), 470 nm (c), and 730 nm (d), respectively, where the blue solid curve is from the sinusoidal pulse of one light period, and the red dots are from the monochromatic sources.

To examine the transmission spectrum for the three optimized film thicknesses, we use a sinusoidal wave field of one light period as the incident pulse:

$$e_x^i(x,y,t) = \mathrm{rect}(\frac{t - 0.5T}{T}) E_0 \sin(k_0 y' + \omega_0 t), \tag{2}$$

where rect is the rectangular function. The normalized transmitted energy flux can be defined as

$$P(\omega) = \frac{\pi|y|}{2s} \frac{\mathrm{Re}\{[E_x(0,y,\omega)]^* H_z(0,y,\omega)\}}{\mathrm{Re}\{[E_x^i(0,y,\omega)]^* H_z^i(0,y,\omega)\}}, \tag{3}$$

#234872 - $15.00 USD Received 17 Feb 2015; revised 27 Mar 2015; accepted 31 Mar 2015; published 9 Apr 2015

where the Fourier transform

$$F(\omega) = \int_0^{t_f} f(t) \exp^{-i\omega t}\, dt \tag{4}$$

is used for the simulated and incident fields. The obtained energy flux $P(\omega)$ as a function of wavelength λ is shown in Fig. 2(b), 2(c), and 2(d) for $h = 205$ nm, 470 nm, and 730 nm, respectively. The wavelengths yielded at corresponding peak transmission are 569 nm, 564 nm, and 560 nm, respectively. At $\lambda = \lambda_0$, the normalized energy fluxes are 4.28, 4.27, and 4.28, respectively, which are in good agreement with those obtained in Fig. 2(a). To verify the spectra, we also use monochromatic sources with its wavelength λ from 400 nm to 700 nm in a step of 10 nm to obtain the normalized energy flux. The results are shown in Fig. 2; they coincide with those from the incident pulse.

We further show in Fig. 3 the history of the transmitted electric fields observed at the location $(0, -\lambda_0)$ for the three optimized film thicknesses from the monochromatic source of wavelength λ_0. We find that when $h = 205$ nm, the amplitude is monotonically increased to a constant within a few periods; when the film is thicker, the field is periodically modulated, and it takes a longer time to saturate. For $h = 470$ nm and 730 nm, the modulation periods are $2T$ and $3T$, respectively, while the amplitudes at saturation are similar. We believe that the monotonic increment and periodical modulation in the transmitted fields result from the Fabry-Pérot-like resonance.

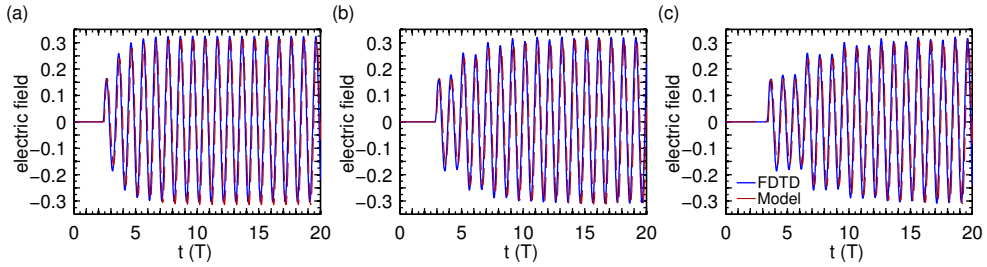

Fig. 3. The history of the electric fields at $(0, -\lambda_0)$ from the simulation (solid blue curve) and the modeling result of $M = 20$ and $N = 10$ (dashed red curve), where $h = 205$ nm (a), 470 nm (b), and 730 nm (c), respectively.

3. Analytical model based on Fabry-Pérot-like resonance

Despite the fact that it is a continuous wave source, we discretize the wave field generated in each light period as an individual unit. The electric field in the x-direction of the m'th wave unit at the source location $(x, h+d)$ is given as

$$e_x^m(t) = E_0 \text{rect}(\frac{t - t_m}{T}) \sin(\omega_0 t), \tag{5}$$

where m is a positive integer, and $t_m = (2m-1)T/2$ is the middle time of the m'th unit.

Each wave unit propagates to the film surface in the time of d/c_0 after generated. It is partially transmitted through the slit entrance interface. The unit peak is delayed and amplified due to the accumulation of the surface charges to draw adjacent energy into the slit as the so-called funnel effect [18, 24]. When the transmission coefficient is τ_{ab}, the time-delay and the amplification ratio are $[\arg(\tau_{ab})/(2\pi)]T$ and $|\tau_{ab}|$, respectively. The transmitted unit propagates to the slit exit in the time of $(h/\lambda_s)T$, where $\lambda_s = 0.94\lambda_0$ is the wavelength in the slit measured from our FDTD simulation (the wavelength shift will be discussed later). Then, it will be partially

#234872 - $15.00 USD Received 17 Feb 2015; revised 27 Mar 2015; accepted 31 Mar 2015; published 9 Apr 2015

transmitted out through the exit interface as the first subunit, $n = 1$, where n is the index of subunit. The charge accumulation at the exit surface delays the peak by $[\arg(\tau_{bc})/(2\pi)]T$ and amplifies the subunit by a ratio of $|\tau_{bc}|$, where τ_{bc} is the transmission coefficient at the exit. After exiting the slit, the subunit diffracts as a cylindrical wave in the area c and reaches the observation location $(0, y)$ in the time of $|y|/c_0$. Thus, the middle time for the $n = 1$ subunit to propagate from the source location to the observation location is $t_{m1} = t_m + d/c_0 + t_s + |y|/c_0$, and its amplitude is $E_{m1}(y) = \alpha(y)E_0|\tau_{ab}\tau_{bc}|$, where $t_s = [\arg(\tau_{ab})/(2\pi)]T + (h/\lambda_s)T + [\arg(\tau_{bc})/(2\pi)]T$ and $\alpha(y)$ is the decay coefficient of the field due to diffraction.

Besides exiting from the slit, the unit is partially reflected at the exit interface and travels back. Then, it is reflected at the entrance interface and propagates toward the exit again. The corresponding time-delay and amplitude decay due to reflection are $[\arg(\rho_{abc})/(2\pi)]T$ and $|\rho_{abc}|$, respectively, where ρ_{abc} is the coefficient of the two reflections. The time of the round trip is estimated as $t_{rt} = (2h/\lambda_s)T + [\arg(\rho_{abc})/(2\pi)]T$. Then, the unit will be partially transmitted through the exit interface as the second subunit (i.e., $n = 2$) and partially reflected again at the exit interface. The middle time for the $n = 2$ subunit to arrive at the observation location is thus $t_{m2} = t_m + d/c_0 + t_s + t_{rt} + |y|/c_0$, and the amplitude is $E_{m2}(y) = \alpha(y)E_0|\tau_{ab}\rho_{abc}\tau_{bc}|$. This process repeats when the wave unit delivers more subunits, which is similar to what is considered in the Fabry-Pérot-like resonance [18, 19].

The middle time of the n'th subunit to arrive at the observation location is

$$t_{mn} = t_m + d/c_0 + t_s + (n-1)t_{rt} + |y|/c_0, \tag{6}$$

while the amplitude is

$$E_{mn}(y) = \alpha(y)E_0|\tau_{ab}\rho_{abc}^{n-1}\tau_{bc}|. \tag{7}$$

We assume that the field of the subunit maintains the ideal sinusoidal shape of one light period. Thus, the electric field of the n'th subunit of the m'th wave unit is given as

$$e_x^{mn}(y,t) = \mathrm{rect}(\frac{t - t_{mn}}{T})E_{mn}(y)\sin[\omega_0(t - t_{mn} + T/2)]. \tag{8}$$

According to the superposition principle, the field of subunits produced by each wave unit can be summed. Therefore, the observed electric field is

$$e_x(y,t) = \sum_{m=1}^{M}\sum_{n=1}^{N} e_x^{mn}(y,t), \tag{9}$$

where M (N) is the maximum number of the wave unit (subunit) included.

The decay coefficient $\alpha(y)$ can be obtained from the energy conservation after the wave amplitude is saturated. The time-averaged Poynting vector in the y-direction at the location $(0, y)$ is

$$S(y) = \frac{E^2(y)}{|Z(y)|}\frac{1}{T}\int_{t_f - T}^{t_f}\sin(\omega_0 t)\sin\{\omega_0 t - \arg[Z(y)]\}dt, \tag{10}$$

where $E(y)$ is the amplitude of the observed field in Eq. (9), and $Z(y)$ is the complex impedance. The energy flux propagating through the slit should be equal to that through the semi-circumference $\pi|y|$ at $y \ll 0$. Thus, we have

$$2sS(0) = \pi|y|S(y). \tag{11}$$

Therefore, the decay coefficient by the definition is

$$\alpha(y) \equiv \frac{E(y)}{E(0)} = \sqrt{\frac{2s}{\pi|y|}\frac{|Z(y)|}{|Z(0)|}\frac{\cos\{\arg[Z(0)]\}}{\cos\{\arg[Z(y)]\}}}. \tag{12}$$

#234872 - $15.00 USD Received 17 Feb 2015; revised 27 Mar 2015; accepted 31 Mar 2015; published 9 Apr 2015

Note that Eq. (12) is valid only for $y \ll 0$.

The interference between exiting wave units in our model is similar to the multiple scattering formalism [25]. However, our model is an initial value problem in time domain while the multiple scattering is a boundary value problem in spatial domain.

4. Model parameters obtained from FDTD simulation

A slit in a film of thickness $h = 10\ \mu$m is simulated to obtain the parameters needed by the model. Figures 4(a) shows the history of the simulated electric field at the entrance center of the slit. Because $d = \lambda_0$, the phase zero of the first unit arrives at $t = T$. However, the observation is made at the arriving time of the field peak (i.e., the phase $\pi/2$). Since the phase $\pi/2$ and the peak is $0.25T$ after the phase zero, the peak arrives at $1.25T$. With the film presented, we observe that the arriving time of the peak is $1.31T$, as listed in Table 1. Hence, the phase shift is $\arg(\tau_{ab}) = (1.31T - 1.25T) \times (2\pi/T) = 0.12\pi$. The transmission time-delay remains constant for all wave units.

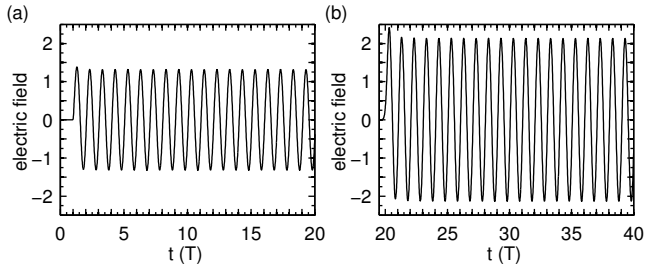

Fig. 4. The history of the simulated electric field at the centers of the entrance (a) and the exit (b) from the simulation of $h = 10\ \mu$m.

Table 1. The time of first five peaks arriving at the centers of the entrance and the exit as well as their corresponding electric field amplitudes obtained from the simulation of $h = 10\ \mu$m.

	At entrance center		At exit center	
m	$t\,(T)$	amplitude	$t\,(T)$	amplitude
1	1.31	1.38	20.31	2.42
2	2.31	1.32	21.31	2.16
3	3.31	1.32	22.32	2.14
4	4.31	1.32	23.31	2.13
5	5.31	1.32	24.31	2.13

The first amplitude is larger than unity, as shown in Fig. 4. Then, the following amplitudes are slightly decreased and remain constant. The amplitude at steady is used to calculate the amplification ratio. As listed in Table 1, we obtain $|\tau_{ab}| = 1.32$.

Figure 4(b) shows the electric field at the exit. The first peak arrives at $t = 20.31T$, as listed in Table 1. Hence, the phase shift at the exit interface is $\arg(\tau_{bc}) = [20.31T - d/c_0 - (h/\lambda_s)T - 0.25T] \times (2\pi/T) - \arg(\tau_{ab}) \simeq 0.01\pi$.

Compared with that at the entrance, the electric field is further increased at the exit. The amplitude at steady is used to calculate the amplification ratio, i.e., $|\tau_{bc}| = 2.13/|\tau_{ab}| = 1.61$.

The simulation shows that the magnetic field peak arrives $0.17T$ before the peak of the electric field, and the steady amplitude is 1.10 (not shown). The impedance at the exit is thus

#234872 - $15.00 USD Received 17 Feb 2015; revised 27 Mar 2015; accepted 31 Mar 2015; published 9 Apr 2015

estimated to be $Z(0) = (2.13/1.10)\exp[i(-0.17)\times 2\pi] = 1.94\exp(-i0.34\pi)$. The impedance at the observation location is $Z(-\lambda_0) = 1.01\exp(-i0.06\pi)$.

The reflected wave cannot be easily separated from the incident wave because of the interference. For the case of $h = 205$ nm, the transmitted electric field amplitude at the early stage is monotonically increased due to the constructive interference condition $t_{rt} = T$ and $t_{mn} = t_{m'n'}$ if $m+n = m'+n'$, where m' and n' are positive integers. Since

$$t_{rt} = \frac{2h}{\lambda_s} + \frac{\arg(\rho_{abc})}{2\pi} = 1, \tag{13}$$

we obtain $\arg(\rho_{abc}) \simeq 0.44\pi$. The peak at $y = 0$ yielded from Eq. (9) for $M \gg 1$ can be simplified as

$$e_x(0, t_{M1} - T/4) = \alpha(0)E_0|\tau_{ab}\tau_{bc}|(1 + |\rho^1_{abc}| + |\rho^2_{abc}| + \cdots + |\rho^{M-1}_{abc}|), \tag{14}$$

where $\alpha(0) = 1$ by the definition. The peak value obtained from the simulation is 4.12 for $M = 10$ (not shown) so that $|\rho_{abc}| \simeq 0.48$.

5. Modeling results and comparison with simulation

The results yielded from Eq. (9) for the $m = 1$ wave unit and $N = 10$ are shown in Fig. 5, where h is selected for optimizing the transmission. All their round-trip times are close to a multiple of T. For the $h = 205$ nm case, $t_s \simeq 0.46T$, $t_{11} = t_1 + d/c_0 + t_s + |y|/c_0 \simeq 2.96T$, $t_{1n} = t_{11} + (n-1)t_{rt}$, where $y = -\lambda_0$ and $t_{rt} = T$. In this case, the end of the $n = 1$ subunit coincides with the beginning of the $n = 2$ subunit which just finishes a round trip; but, the amplitude of the later is decreased by the factor of $|\rho_{abc}|$. At the end of the $n = 2$ subunit, the $n = 3$ subunit begins, and its amplitude is further decreased by one more factor of $|\rho_{abc}|$. This repeats till it fades out, as shown in Fig. 5(a).

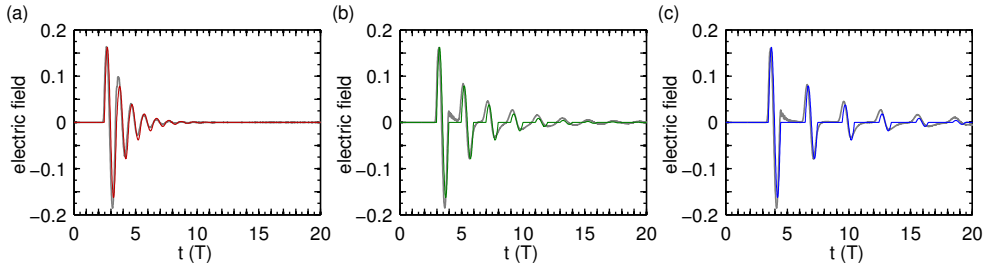

Fig. 5. The history of the electric field at $(0, -\lambda_0)$ of the wave unit $m = 1$ obtained from the model, where $N = 10$, $h = 205$ nm ($t_{rt} = T$) (a), 470 nm ($t_{rt} \simeq 2T$) (b), and 730 nm ($t_{rt} \simeq 3T$) (c), respectively. The grey curves show the history of the electric field from the sinusoidal pulse of one light period, while the colored curves are from a continuous sinusoidal wave source.

For the $h = 470$nm case, $t_s \simeq 0.96T$, $t_{11} \simeq 3.46T$, and $t_{rt} \simeq 2T$ because h is almost $0.5\lambda_s$ thicker than 205 nm. As shown in Fig. 5(b), after the $n = 1$ subunit ends, there is a gap of about one T because the $n = 2$ subunit is still in its round trip. Then, it arrives with the middle time $t_{12} \simeq 5.46T$. The $n = 3$ subunit arrives with the middle time $t_{13} \simeq 7.46T$. This also repeats till the field fades out. For the $h = 730$ nm case, t_s, t_{11}, and t_{rt} are further increased approximately to $1.46T$, $3.96T$, and $3T$, respectively, while the gap width is about $2T$, as shown in Fig. 5(c). In these two later cases, the fading time is longer than the first case of $h = 205$ nm. The history of the simulated electric fields from the sinusoidal pulse of one light period passing through these films are shown in Fig. 5. The simulation results (e.g., the repeating subunits) generally agree with those from the modeling.

#234872 - $15.00 USD Received 17 Feb 2015; revised 27 Mar 2015; accepted 31 Mar 2015; published 9 Apr 2015

For a continuous source, the $(m+1)$'th wave unit is one T later than the m'th unit, and so are their subunits. The observed electric field is from the superposition of all units. For all these cases, the $n=1$ subunit of the $m=1$ unit is the first and only one that arrives at the observation location, as shown in Fig. 3. For the $h=205$ nm case shown in Fig. 3(a), $t_{21}=t_{12}$ because $t_{rt}=T$. The second arriving period of the observed field is from the in-phase interference between the $m=2, n=1$ subunit and the $m=1, n=2$ subunit. The amplitude is thus increased by $|\rho_{abc}|$. Then, the $m=3$, $n=1$ subunit arrives at the next period, i.e., $t_{31}=t_{22}=t_{13}$. Since the amplitudes of the subunit of the $m=2$ and $m=1$ units have decayed by $|\rho_{abc}|$ and $|\rho_{abc}|^2$, respectively, the observed field amplitude has been increased by $|\rho_{abc}|+|\rho_{abc}|^2$. The in-phase interference continues till the amplitude saturates.

For the $h=470$ nm (i.e., $t_{rt}\simeq 2T$) case shown in Fig. 3(b), the $m=2$, $n=1$ subunit with the same amplitude as the $m=1, n=1$ subunit fills the first temporal gap after the later's end while there is no overlapping with other subunits. This makes the first modulation period of $2T$. At the third period of the observed field, the $m=1$, $n=2$ subunit, the first gap of the $m=2$ unit, and the $m=3$, $n=1$ subunit overlap; that is, $t_{31}=t_{12}$. While, at the forth period, the second gap of the $m=1$ unit, the $m=2$, $n=2$ subunit, the first gap of the $m=3$ unit, and the $m=4$, $n=1$ subunit overlap; that is, $t_{41}=t_{22}$. Both resultant amplitudes of the observed field are increased by $|\rho_{abc}|$ and has the second modulation period of $2T$. The amplitude of the third $2T$ modulation is further increased by $|\rho_{abc}|^2$ because $t_{51}=t_{32}=t_{13}$ and $t_{61}=t_{42}=t_{23}$. The increment occurs at every $2T$ till the amplitude saturates. As for the $h=730$ nm case whose $t_{rt}\simeq 3T$, as shown in Fig. 3(c), the modulation period is $3T$ due to the similar reason. In fact, we can further obtain the relation that $t_{mn}=t_{m'n'}$ if $m+pn=m'+pn'$, where p is the number of wave period in one round trip and also the resultant modulation period, e.g., $p=1$ for $h=205$ nm, $p=2$ for $h=470$ nm, and so on. The modeling results agree well with the corresponding FDTD simulation results, as shown in Fig. 3.

6. Discussion

The wavelength in the slit λ_s shifted from λ_0 is a numerical issue in FDTD simulation. In our case, $\lambda_s=0.94\lambda_0$, $0.97\lambda_0$, and $0.98\lambda_0$ when the cell sizes are 5 nm, 2.5 nm, and 1.25 nm, respectively. The difference $(\lambda_0-\lambda_s)$ is much greater than the cell size resolution. Although it could vanish if the cell size approached to zero, the wavelength shift is inevitable since the cell size is always finite. We are currently developing a new numerical scheme; but, this is beyond the scope of this article. Nevertheless, this wavelength shift does not affect the physical issues of concern here because the resultant shifts of all relevant quantities (e.g., v, h, t_s^{-1}, or t_{rt}^{-1}) in the model are linearly dependent on λ_s so that their effects are canceled.

We have shown that the modeling results from the $m=1$ wave unit generally agree with those from the simulation of the single sinusoidal pulse in Fig. 5. Therefore, this study could be applied to the photonics of ultrashort pulse lasers. Suppose that the temporal full-width at half-maximum of its intensity is defined as Δt. When $\Delta t \geq t_{rt}$, the subunits partially overlap so that the temporal width of the observed field is effectively increased to be larger than that of the incident pulse [22]. When Δt is short enough (e.g., $\Delta t \ll t_{rt}$), the whole pulse could be seen as a wave unit, and the subunits can barely interfere with each other. Therefore, the observed field will be a train of pulses with decaying amplitude, as implied in Fig. 5.

In structured PEC, spoof SPs could lead to wave dispersion [14]. For a real metal, SPs can be excited, and the plasmonic effect including both structural parameters and frequency-dependent dielectric functions can disperse the wave [26]. However, since similar Fabry-Pérot-like resonance exists in the case of real metal [18], we believe that the key physics revealed by our modeling should still be valid.

#234872 - $15.00 USD Received 17 Feb 2015; revised 27 Mar 2015; accepted 31 Mar 2015; published 9 Apr 2015

7. Summary

In summary, we have verified Fabry-Pérot-like resonance for the single slit configuration by demonstrating the periodical variation of the transmitted energy as a function of thickness and transmission spectra with the monochromatic or pulse sources. A new analytical model was proposed to study the modulated light transmission through a subwavelength slit at early stage, as obtained by our FDTD simulation. Each wave unit in the model produces a train of subunits with decaying amplitudes. The temporal gap between the subunits depends on the round-trip time of the wave traveling in the slit, which are verified by the simulation of the incident sinusoidal pulse. When the wave units are continuous, the observed field amplitude of the transmitted light is monotonically increased till saturation while the round-trip time is equal to one light period as determined by the film thickness. When the round-trip time is a multiple of one light period, the temporal gap is filled by the following wave unit(s) to form the modulation. The modulation period is equal to the round-trip time while the gap time is one light period less. The modeling results agree well with those obtained from the FDTD simulation. The resultant shifts of all relevant quantities in the model due to the wavelength shift does not affect the physical issues of concern here. Possible applications for those with pulsed laser and the plasmonic effect are discussed.

Acknowledgments

The authors are grateful for the support of Ministry of Science and Technology, Taiwan, R.O.C. and the computing resources at the National Center for High-Performance Computing.

#234872 - $15.00 USD Received 17 Feb 2015; revised 27 Mar 2015; accepted 31 Mar 2015; published 9 Apr 2015